

Abstract

Theoretical condensed matter research is plagued by a fundamental issue of complexity. The sheer amount of degrees of freedom in a material on any technologically relevant scale is overwhelming (e.g. $\sim 10^{23}$ electrons per cm^3), and makes it impossible to describe the quantum mechanical wavefunction exactly.

The Hamiltonian plays a central role in the description of crystals, the subject of this thesis. It can be decomposed into various parts, and their interactions. Depending on the physics under scrutiny it then often suffices to solve only one of those parts. This can be either because the energy scales and associated timescales that govern the constituents are very different, or because the interactions between them are small. One example, often put into practice, is the separation of electronic and phononic (lattice) degrees of freedom, leading to the well-known Born-Oppenheimer approximation, decoupling their respective motion. Another is the often neglected spin-orbit coupling, due to the tiny prefactor associated with its relativistic origin.

Solving these subproblems then allows for progress to be made in understanding the physics that govern them. However, there will inevitably be systems for which this interaction is not small and leads to physics that manifestly depends on both subsystems combined. In this thesis we focus on these cases and how they arise in functional materials, with the occasional eye towards applications in technology.

The reason why these cross-order couplings can be interesting for technological applications, is that often one of the orders is more robust with respect to perturbations, and therefore more long-lived, but also harder to control efficiently. By exploiting the cross-order coupling in certain materials, one could theoretically control the long lived order by applying perturbations to the more easily controllable order.

In giant Rashba effect systems, the coupling between spin and ferroelectric order leads to a linear spin-splitting of the band structure, whose sign depends on the orientation of the ferroelectric polarization. We show that, rather than the relativistic Rashba effect, a combination of electrostatics and atomic spin-orbit coupling lies at the origin of the large splitting. The coupling between magnetism and ferroelectricity in multiferroic GdMn_2O_5 leads to a peculiar four-state hysteresis loop for the ferroelectric polarization, which depends on the magnitude, angle and history of the applied magnetic field. As we will show, this four-state hysteresis loop is accompanied by a full 360° rotation of spins in the material, which resembles the crankshaft of a car, converting the linear back-and-forth motion of the magnetic field into a rotational motion of the spins. In a thin film of elemental Chromium, the ultrafast dynamics of a spin density wave, coupled to a slower varying charge density wave, allows for a high

degree of control of the latter through excitations of the former. This allows us to predict the sequence of optical pulses to be applied to the material in order to follow closely an enveloping signal function. And finally, the coupling between ferroelectricity and strain in BaTiO₃ leads to a softening at purely ferroelectric domain walls, allowing for some mechanical control of the position of this wall.

We utilize both theoretical and computational tools to understand the nature of these interactions, how they lead to cross-order coupling in these materials, and how this then translates into the experimentally observed behavior.

Acknowledgements

Contents

Chapter 1

Coupling between spin and strain density waves

1.1 Introduction

Chromium is an itinerant antiferromagnetic metal. It is the hallmark example of a material where a SDW develops due to local repulsive interactions of the electron gas, combined with a nesting of the fermi surface.

1.2 Experimental methods

Before focusing on the theoretical description of the coupling between the SDW and CDW, we take a look at the experimental techniques and results that we are seeking to reproduce. Optical pulses were used to heat up the material, mostly absorbed by the SDW order through photoexcitation. An x-ray free-electron laser (XFEL) is then used to probe the bragg-peaks of the CDW and how they change in time. The need of the XFEL can be attributed to the very short timescales at which the observed behavior is exhibited by the material, with resolutions of a couple femtoseconds being made accessible. The scattering intensity of the bragg peak is directly proportional to the magnitude of the CDW, offering both phase and amplitude information of the oscillation that we study. It is important to realize that the SDW order is not directly accessible through these kinds of measurements, so we are effectively studying the effect of exciting one order parameter through the reaction of the other due to the coupling between them. XFELs also allow for higher peak selectivity (narrow and intense satellite Bragg peaks), such that it allows for measurements performed on thin films even deposited on thick substrates, as was the case in the experiments performed by A. Singer et.al. The thin films offer a clarity in terms of describing the physics of this process, since it leads to a very even excitation of the entire volume, and it causes the order parameters to be homogeneous throughout the material. This absence of topological defects is confirmed by the absence of a widening of the satellite peak associated with the PLD, as compared with the peaks of the material itself. [not sure about this, I actually don't understand what they are talking about in the paper either]. To this end,

a 30nm thick Cr film was used in the experiments, harboring seven periods of the SDW perpendicular to the plane. This thinness of the film also decreases the Neel temperature to 290K, from the bulk value of around 307K. The pulses used to excite the SDW were 40 fs long, with a total intensity of 2.9 mJ/cm^2 . In the experiments with two sequential pulses the power of the second pulse was roughly half that of the first.

1.3 Theory

[some explanation of Peierls instabilities etc, the things that cause the SDW in the first place?]

The geometry that is used in the experiment is such that a microscopic model as described above is unnecessary to describe the essential physics, since the Cr thin film can be considered to be homogeneous throughout the experiment. This allows us to instead adopt a continuum description utilizing a standard Landau theory with two order parameters describing the SDW (L) and PLD (y) and a coupling between them to describe the magnetostriction.

$$F(L, y, T_L) = \frac{\alpha}{2}(T_L - T_c)L^2 + \frac{\beta}{4}L^4 - gL^2y + \frac{\omega_0}{2}y^2 + \frac{b}{4}y^4, \quad (1.1)$$

where L , y and T_L are the time dependent variables. The double well potential that leads to the SDW is characterised by α and β , with the temperature of the SDW given by T_L , with the critical temperature T_c below which the phase transition occurs and the SDW order sets in. The coupling between the two order parameters is given by term with γ . Only even orders of L appear in the energy, since the energy is time reversal even, but L is time reversal odd. The PLD order parameter y has a zero equilibrium value without any interaction with L , since it is not the primary order parameter. The fourth order term $\frac{b}{4}y^4$ is only included to provide a better fit to some of the anisotropic features of observed by the experiment, not to bound the energy potential in terms of y , as would be required if y was the primary order parameter with a negative second order term. It is the interaction with the primary order parameter L that provides the “force” to move y up in its own potential, leading to the nonzero equilibrium value. This concept is the key to understanding the observed physics.

Since SDWs in Chromium originate purely from electronic correlations, it is fair to equate the temperature of the SDW order parameter with the electronic temperature. It is also known that the electronic excitations caused by the X-rays that were used in the experiments thermalize on a very short timescale, allowing us to treat them thermodynamically and assign a temperature [Nicholson2016]. For our modeling the X-ray pulses thus effectively inject heat into the SDW, which then thermalizes with the lattice (a phonon bath) on a longer timescale of the order of 400 ps. This naturally leads to a two temperature model to describe the perturbation caused by the pulses, with T_L the temperature for the SDW and T_b the temperature for the phonon bath:

$$\begin{aligned} c_L \dot{T}_L &= -k(T_L - T_b) + q \\ c_b \dot{T}_b &= -k(T_b - T_L). \end{aligned} \quad (1.2)$$

c_L, c_b are the heat capacities of the SDW and the bath, k the heat transfer rate, and q signifies the heat injected into the system through the photon pulses,

and is modeled by a time dependent gaussian $q(t) = \frac{f}{\tau\sqrt{2\pi}}e^{-\frac{1}{2}\left(\frac{t-t_0}{\tau}\right)^2}$, where τ denotes the pulse width and f the fluence. The dots signify time derivatives.

The time evolution of the system can be described using the Langrangian:

$$\mathcal{L}(L, y, \dot{L}, \dot{y}, t) = \frac{m_L \dot{L}(t)^2}{2} + \frac{m_y \dot{y}(t)^2}{2} - F(L, y, t), \quad (1.3)$$

with associated Euler-Lagrange equations:

$$\begin{aligned} \frac{\partial \mathcal{L}}{\partial L} - \frac{d}{dt} \frac{\partial \mathcal{L}}{\partial \dot{L}} &= \gamma_y \dot{L} \\ \frac{\partial \mathcal{L}}{\partial y} - \frac{d}{dt} \frac{\partial \mathcal{L}}{\partial \dot{y}} &= \gamma_L \dot{y} \end{aligned} \quad (1.4)$$

where the γ denote the damping parameters for both order parameters. Substituting Eq. ?? leads to

$$\begin{aligned} m_L \ddot{L} &= -\alpha(T_L - T_c)L - \beta L^3 - \gamma_L \dot{L} + 2gLy \\ m_y \ddot{y} &= -\omega_0^2 y - b y^3 - \gamma_y \dot{y} + gL^2. \end{aligned} \quad (1.5)$$

These equations, together with Eqs. ?? describing the temperature evolution of the SDW (T_L) under influence of the optical pulses, fully describe the dynamics that are experimentally observed. One obvious remark can be made here, in that to be completely exact, the energy dissipated through the damping terms in Eq. ?? should be absorbed into the bath and thus influence T_b . However, the case can be made that since these are only single modes, their contribution to the heating of the bath will be negligible compared with that coming from the thermalization of all the electronic degrees of freedom.

1.4 Methods

To solve the time evolution of L and y throught the differential equations in Eqs. ?? we used the numerical integration methods implemented in the DifferentialEquations.jl package. More specifically the [I think Tsit5] algorithm was used. Originally the dynamics were fully solved both for L and y , but it was found during the fitting process that the dynamics of L are significantly faster than those of y , i.e. both the “mass” of the SDW order is orders of magnitude smaller than that for y parameter, and the parameters describing the Landau free energy potential are orders of magnitude larger. This all leads to the SDW almost perfectly tracking its instantaneous minimum on the timescales that are of interest. Solving dynamics with significantly different timescales is in general hard from the numerical point of view, and while there are other ways around this, we opted to take $m_L = 0$ and use the instantaneous minimum in the equation describing the dynamics of y . This minimum is found by minimizing the Landau free energy in Eq. ?? for a given y and T_L in terms of L such that $\frac{\partial F}{\partial L} = 0$, leading to:

$$L(t) = \pm \sqrt{\frac{-\alpha(T_L - T_c) + 2gy}{\beta}}. \quad (1.6)$$

The starting temperature of the bath was fixed at 115 K, and T_c was observed to be at 290 K, consistent with previous observations that in general the Néel temperature of a thin film is lower than that of the bulk material (bulk Cr has a Néel temperature of ≈ 310 K). Most parameters of the model described above were not known a priori and thus had to be fitted to the experimental measurements. To aid with the fitting, judicious starting values could be chosen for some parameters. For example, it was known that the pulse width τ was under 100 fs, the oscillation frequency of the PLD $\omega_0 \approx 14$ or equivalently a period of around 450 fs. It was also known that in general the second pulse had a fluency of around 80% that of the first, and we also chose the initial heat capacities for the bath and electronic degrees of freedom to have a ratio $\frac{c_b}{c_L}$ close to 7, which was known from previous experiments [citation].

For each set of trial parameters, the time evolution of the system was solved on an interval of -2 ps to 8 ps, where the lower bound is chosen so that the numerical integration starts from a completely equilibrium initial condition. This is needed because when the sharp pulse arrives around 0 ps, some energy already enters the system slightly before 0 ps due to the gaussian shape. The error of the solution \tilde{x} w.r.t. the experimental measurements x is then the mean square sum $err = \sum_{i=1}^n \frac{(x_i - \tilde{x}_i)^2}{n}$, where i denote the measurement points. The numerical optimization was done through the Optim package, where it was found that the Nelder Mead simplex algorithm [citation needed] works best for this very non-linear problem.

1.5 Results

The experimental results we use as a basis to fit our model to are shown in Fig. ???. In the numerical model, we found in earlier trials that the dynamics of the SDW order parameter L is orders of magnitude faster than the ones from the PLD y , as expected. This can also be seen from Fig. ?? since the energy potential is a lot flatter for y than for L , leading to a slower time evolution. This difference in dynamics makes it extremely hard to solve the differential equations numerically, we therefore assumed that at each timestep the L order parameter is in equilibrium in its instantaneous energy potential. This is equivalent to the limit of the mass m_L in Eq. ?? going to zero. The value of L at a given T_L and y can be found by minimizing the Landau free energy ??

$$L_0 = \pm \sqrt{\frac{\alpha(T_L - T_c) + 2gy}{\beta}}. \quad (1.7)$$

This eliminates to evaluate Eq. ??, instead using Eq. ?? to evaluate L in the partial differential equation for the evolution of y .

We then took eleven representative experiments, which can be thought of as horizontal slices of Fig. ??(a), in order to fit the model parameters to get the best total fit accross all datasets. The parameters are

$$\alpha = 6039, \beta = 7.97 \times 10^7, g = 0.52, \gamma_L = 25.0, \quad (1.8)$$

$$\omega_0 = 14.1, b = 3.38 \times 10^8, \gamma_y = 0.76, \quad (1.9)$$

$$f = 64.43, c_b = 3.58, c_L = 0.36, k = 1.29, \tau = 0.074 \quad (1.10)$$

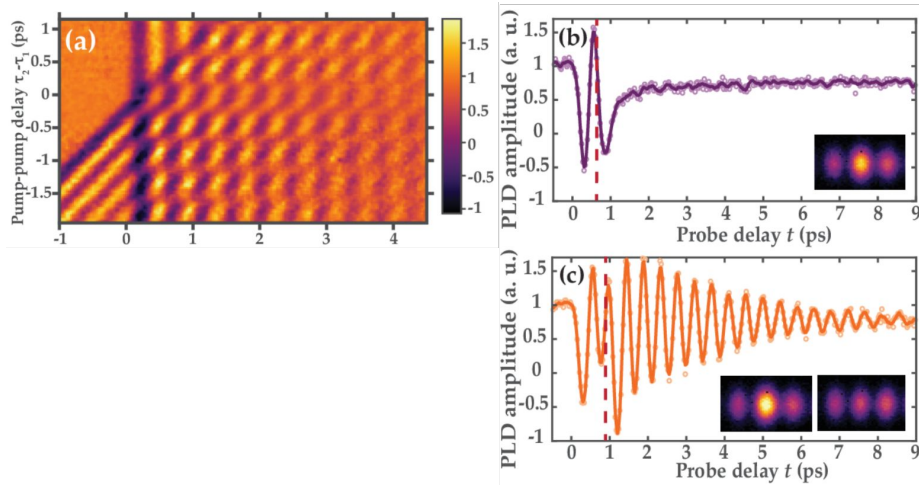


Figure 1.1: Experimental measurements. (a) Heatmap showing different pump-pump delay experiments. Notice the low intensity horizontal band around 0 ps pump-pump delay, where the oscillation amplitude is not at the maximum due to only one big pulse exciting the material and heating it through the phase transition, thus wasting a portion of the energy. The horizontal bands with alternating maximum and minimum magnitudes highlight constructive and destructive interference. (b-c), Magnitude of the strain wave in two extreme control cases, where (b) showcases maximum destructive interference, and (c) close to maximum constructive interference. Solid lines are experimental data (empty circles in figure) smoothed by a Savitzky-Golay filter. b – pump-pump delay of 620 fs, c – pump-pump delay of 845 fs.

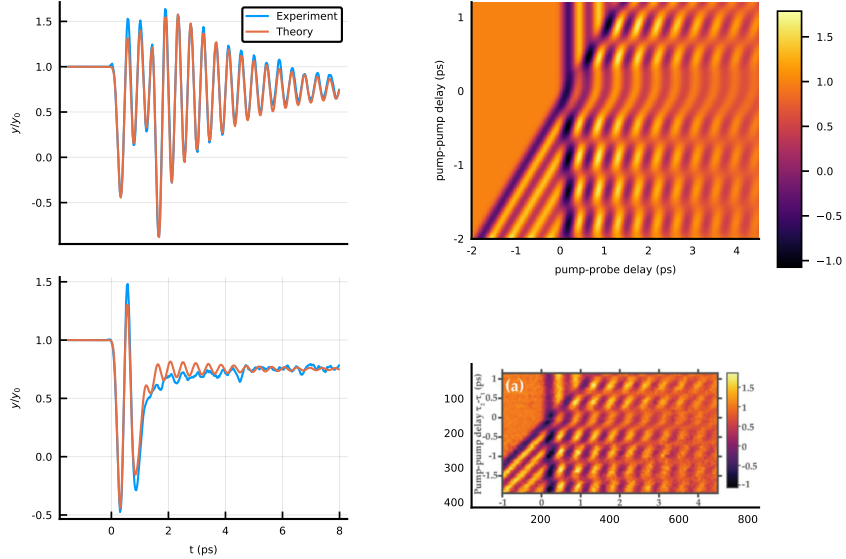


Figure 1.2: Comparison of theoretical fit vs Experiment. (a-b) Two examples of fits to constructive (a) and destructive (b) experiments. (c-d) Comparison of the theoretically generated heatmap (c) with the experimental heatmap (d).

The results of this fitting procedure is shown in Fig. ??, showing an excellent agreement between the theory and experiment.

To get a deeper understanding of the underlying effect, we look at the evolution of the free energy surfaces for both order parameters, as shown in Fig. ???. The characteristic double well potential for $L \neq 0$ equilibrium is clearly visible, and as expected, when the pulses hit and T_L increases in the term $\alpha(T_L - T_c)L^2$ of Eq. ??, we see that the potential flattens causing the the minimum of L to very quickly change, as discussed above. This in turn causes the single-well potential of y to shift as quickly. The dynamics of y is orders of magnitude slower than that of L and due to this instant shift of the energy surface, it will cause an oscillation of y . While the temperature T_L decreases again, L and the minimum of the y potential shift back towards the original equilibrium position. The oscillation of y remains for a relatively long time while this shift is occurring since the damping is not that big (of the order of 4ps). It then becomes clear that if the second pulse can repeat this mechanism while the oscillation of y is still there, it can be increased or decreased depending on the timing. Having this understanding, let's investigate what the ideal way to excite y is.

First of all, when the system is relatively close to the phase transition of L , a small increase of temperature causes a large change in the value of L as shown through Eq. ??, and thus causes a large the shift of the potential for y . It is then important to keep this initial shift of the potential for y in place until y crosses the minimum, converting as much potential energy into "kinetic" energy. This requires L to be heated slightly above the PT, which leads to the largest possible shift of the potential of y , and the additional temperature of L above T_c , together with the non-infinite cooling rate, allows y to gain the maximum kinetic energy.

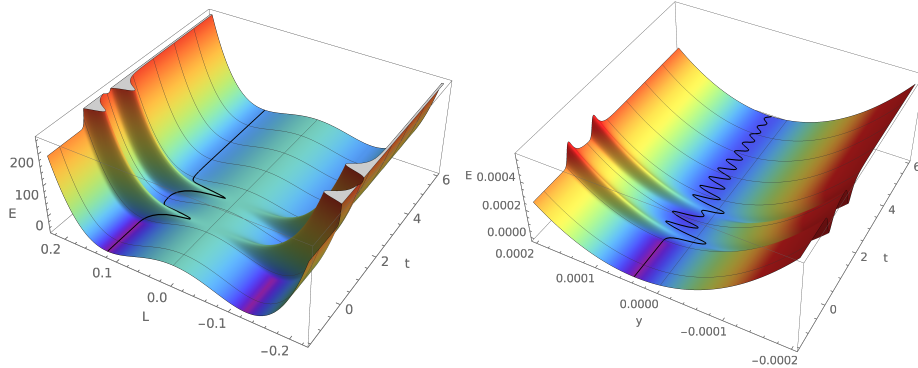


Figure 1.3: Time evolution of the energy surfaces of the order parameters.

Since only the size of L matters for the potential surface of y , it can only cause a shift in one direction, meaning that, similar to someone pushing a swing, the ideal intervals for the subsequent pulses are close to multiples of the period of y , if the goal is maximum oscillation amplitude. The amount of periods depends on the cooling rate of L , this influences how much T_L can cool back down within one period and thus the size of the maximum shift, since this depends on distance of T_L from T_c , and the damping of y since that is the main source of kinetic energy loss. Taking these understandings into consideration, a high degree of control of the oscillation of y can be achieved through the intensity, amount and timing of a pulse train applied to the material. To demonstrate this, we went one step further and utilized the fitted model to simulate what pulse train has to be applied to the material in order for the oscillation maxima to follow a given envelope signal. To limit the dimensionality of the manifold of possible solutions, we performed the following ruleset:

- Only one fluence can be used per pulse
- Pulses are grouped in sets per period of oscillation
- The first pulse group only has a single pulse, applied 20 fs after the first non zero value of the envelope function, this determines the fluence of each pulse
- The maximum allowed pulses per group is fixed
- The groups are then fitted sequentially, since the later pulses don't influence the oscillation caused by the earlier ones
- If the function is seen to increase during a period, the pulses will be initiated close to the ideal boost location, and if a decrease is required, close to the ideal brake location

Adhering to these rules, we tested this procedure on different envelope functions, showcased in Fig. ???. One assumption made here was that the heat capacity of the bath c_b was increased to infinity, this is done because with the increase of temperature of the bath, the equilibrium position of L changes and

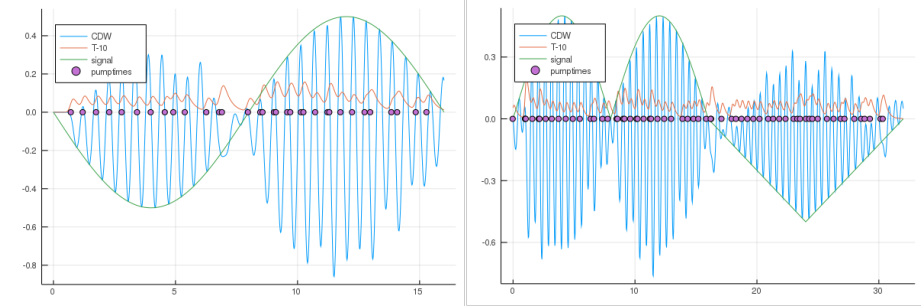


Figure 1.4: Two examples of optimal control. (a) Shows a reproduction of a sinusoidal envelope function, (b) shows the result for more complicated envelope, with an absolute value of a sinusoidal followed by a half a period of a sawtooth function. The pulse train is highlighted by the purple dots, and the evolution of the temperature of the SDW is given by the orange plot.

leads to a general downwards slope of the oscillation of y as see from panel (a-b) of Fig. ??.

Having fit the model, we can go one step further and try to fit the PLD oscillation to an arbitrary signal shape. To this end we use the fitted model, and predict the timing of a fixed fluence pulse train that will result in the required shape. The results are shown in Fig. ?? . This showcases that with an arbitrary pulse train we can achieve indirect, but optimal control of the PLD order parameter.

Bibliography

- [1] J. A. Alonso et al. “A structural study from neutron diffraction data and magnetic properties of RMn₂O₅ (R = La, rare earth)”. In: *Journal of Physics Condensed Matter* 9.40 (1997), pp. 8515–8526. ISSN: 09538984. DOI: 10.1088/0953-8984/9/40/017.
- [2] Sang-Wook Cheong and Maxim Mostovoy. “Multiferroics: a magnetic twist for ferroelectricity”. In: *Nature Materials* 6.1 (2007), pp. 13–20. ISSN: 1476-4660. DOI: 10.1038/nmat1804. URL: <https://doi.org/10.1038/nmat1804>.
- [3] Y. J. Choi et al. “Ferroelectricity in an ising chain magnet”. In: *Phys. Rev. Lett.* 100.4 (2008), pp. 6–9. ISSN: 00319007. DOI: 10.1103/PhysRevLett.100.047601.
- [4] Manfred Fiebig. “Revival of the magnetoelectric effect”. In: *Journal of Physics D: Applied Physics* 38.8 (2005), R123–R152. DOI: 10.1088/0022-3727/38/8/r01.
- [5] Manfred Fiebig et al. “The evolution of multiferroics”. In: *Nature Reviews Materials* 1.8 (2016), p. 16046. ISSN: 2058-8437. DOI: 10.1038/natrevmats.2016.46. URL: <https://doi.org/10.1038/natrevmats.2016.46>.
- [6] E. A. Harris. “Related content EPR of Mn pairs in MgO and CaO”. In: *Journal of Physics C: Solid State Physics* 5 (1972), p. 338.
- [7] Daniel Khomskii. “Classifying multiferroics: Mechanisms and effects”. In: *Physics* 2 (2009), p. 20. DOI: 10.1103/Physics.2.20.
- [8] N. Lee et al. “Giant Tunability of Ferroelectric Polarization in GdMn₂O₅”. In: *Phys. Rev. Lett.* 110 (13 2013), p. 137203. DOI: 10.1103/PhysRevLett.110.137203.
- [9] Yoon Seok Oh et al. “Non-hysteretic colossal magnetoelectricity in a collinear antiferromagnet”. In: *Nature Communications* 5 (2014), pp. 1–7. ISSN: 20411723. DOI: 10.1038/ncomms4201. URL: <http://dx.doi.org/10.1038/ncomms4201>.
- [10] N. A. Spaldin and R. Ramesh. “Advances in magnetoelectric multiferroics”. In: *Nature Materials* 18.3 (2019), pp. 203–212. ISSN: 1476-4660. DOI: 10.1038/s41563-018-0275-2. URL: <https://doi.org/10.1038/s41563-018-0275-2>.

- [11] K. F. Wang, J. M. Liu, and Z. F. Ren. “Multiferroicity: The coupling between magnetic and polarization orders”. In: *Advances in Physics* 58.4 (2009), pp. 321–448. ISSN: 00018732. DOI: 10.1080/00018730902920554. arXiv: 0908.0662.
- [12] S. H. Zheng et al. “Abnormal dependence of multiferroicity on high-temperature electro-poling in GdMn₂O₅”. In: *J. Appl. Phys.* 126.17 (2019). ISSN: 10897550. DOI: 10.1063/1.5120971.